Reverse electric field Monte Carlo simulation for vector radiative transfer in the atmosphere*

Li Xu-You(李绪友), Sun Bo(孙 波)†, and Yu Ying-Ying(于莹莹)

College of Automation, Harbin Engineering University, Harbin 150001, *China*

(Received 24 June 2013; revised manuscript received 31 October 2013; published online 20 April 2014)

In this paper, a reverse electric field Monte Carlo (REMC) method is proposed to study the vector radiation transfer in the atmosphere. The REMC is based on tracing the multiply scattered electric field to simulate the vector transmitted radiance. The reflected intensities with different total optical depth values are obtained, which accord well with the results in the previous research. Stokes vector and the degree of polarization are numerically investigated. The simulation result shows that when the solar zenith angle is determined, the zenith angle of detector has two points, of which the degree of polarization does not change with the ground albedo and the optical depth. The two points change regularly with the solar zenith angle. Moreover, our REMC method can be applied to the vector radiative transfer in the atmosphere–ocean system.

Keywords: radiative transfer, Monte Carlo, atmosphere scattering, polarization

PACS: 42.68.Ay, 05.10.Ln, 42.68.Mj, 42.25.Ja **DOI:** 10.1088/1674-1056/23/6/064219

1. Introduction

The Monte Carlo method is one of the most well-known and widely used numerical methods.[1–3] It is widely used in different fields.[4,5] It is also an effective method for the radiation transfer. Plass *et al.*,[6] Kattawar,[7] Adams and Kattawa,[8] Fischer and Grassl[9] *et al.* simulated the radiation transfer in the atmosphere or atmosphere–ocean system. The standard Monte Carlo method traces a photon beam in a forward direction. A photon beam is emitted and its propagation process is then followed until it is absorbed or leaves the system.[10] However, this method may become extremely inefficient when radiation onto a small spot is desired. Reverse Monte Carlo tracing of photo bundles is known to alleviate this problem. It has been used by several investigators. Meantime, most Monte Carlo methods are based on tracing the Stokes vector $S = (I,Q,U,V)^{\mathrm{T}}$ in simulation. In 2004, Xu[11] proposed a new electric field Monte Carlo simulation and used it to simulate the propagation of polarized light in a turbid medium. The electric field Monte Carlo method is also used to simulate the laser beams[12] and the polarized photon scattering.[13] The electric field Monte Carlo method traces the electric field and phase of light, and easily adapts to the simulation of the propagation of polarized light in the atmosphere. In the polarization navigation, the degree of polarization has a significant influence on the accuracy of polarization navigation.[14] The study of the vector radiative transfer is important for the polarization navigation.

In this paper, we propose an REMC method in which the reverse Monte Carlo method and the electric field Monte Carlo method are utilized to simulate the vector radiative transfer in the atmosphere. The reflected intensities with different total optical depth values are obtained, which accord well with the results in the previous research. Simulation is performed to analyze the influence of the ground albedo and the optical depth on the degree of polarization.

The rest of this paper is organized as follows. In Section 2, we briefly review the basic concepts of radiative transfer, the reverse Monte Carlo method, and the electric field Monte Carlo method. In Section 3, we provide a detailed description of how to use this method in calculations. In Section 4, simulation results are compared with the results of previous research, and the Stoke vector and the degree of polarization are analyzed by employing the REMC. Finally, in Section 5, some conclusions are drawn from the present studies.

2. Theory

The radiative transfer equation (RTE) for randomly-oriented particles passing through a plane-parallel and horizontal atmosphere can be written as[15–17]

$$\hat{s}\nabla \boldsymbol{S}_\lambda(r,\hat{s}) = \boldsymbol{L}_\lambda(\boldsymbol{r},\hat{s}) - \beta_\lambda(\boldsymbol{r})\boldsymbol{S}_\lambda(\boldsymbol{r},\hat{s}) + \frac{\sigma_{s\lambda}(r)}{4\pi}\int_{4\pi}\boldsymbol{S}_\lambda(\boldsymbol{r},\hat{s}')\boldsymbol{\Phi}_\lambda(\boldsymbol{r},\hat{s}',\hat{s})\mathrm{d}\Omega, \quad (1)$$

where $\boldsymbol{S}$ denotes the vector of four Stokes parameters (I,Q,U,V), r the vector pointing to a location, β the extinction coefficient, σ_s the scattering albedo, Φ the phase matrix for scattering, $\hat{s}$ the unit direction vector, and L the intensity of the local radiative source. The Stokes parameters (I,Q,U,V)

*Project supported by the Specific Scientific and Technological Cooperation Between China and Russia (Grant No. 2010DFR80140).

†Corresponding author. E-mail: kylesunbo@hotmail.com

© 2014 Chinese Physical Society and IOP Publishing Ltd

can be defined in terms of the $E_{l,r}$ that are the complex electric field components along parallel and perpendicular directions, respectively, to a meridian plane. The electric field can be defined as follows:[11]

$$E = E_l \boldsymbol{l} + E_r \boldsymbol{r}, \tag{2}$$

where $\boldsymbol{l} \times \boldsymbol{r}$ is in the direction of propagation. The Stokes parameters (I, Q, U, V) can now be defined in terms of $E_{l,r}$ as follows:

$$\begin{cases} I = E_l E_l^* + E_r E_r^*, \\ Q = E_l E_l^* - E_r E_r^*, \\ U = E_l E_r^* - E_r E_l^*, \\ V = \mathrm{i}(E_l E_l^* - E_r E_r^*). \end{cases} \tag{3}$$

We use the electric field Monte Carlo method based on tracing the scattered electric field to simulate the radiative transfer. In the local coordinate system, the scattering of photons is expressed by (m, n, s), where m and n represent the unit vectors along the parallel and perpendicular directions, respectively, to the electric field, and s denotes the propagation direction of the photon.[18] After the current scattering of photons, the propagation direction s' is expressed as

$$s' = m \sin\theta \cos\phi + n \sin\theta \sin\phi + s \cos\theta, \tag{4}$$

where ϕ and θ represent the azimuthal and scattering angles, respectively. The parallel and perpendicular electric fields relative to the current scattering are expressed as

$$\begin{cases} e_l = m \cos\phi + n \sin\phi, \\ e_r = -m \sin\phi + n \cos\phi. \end{cases} \tag{5}$$

The electric field of scattered light is subsequently updated, and given by

$$E' = MRE, \tag{6}$$

where E and E' represent the complex electric field in the previous and present plane, respectively, R denotes the rotation matrix depending on the azimuthal angle ϕ, and M denotes the scattering matrix depending on the scattering angle θ_s.

3. Number calculation method

We model an infinite flat layered atmosphere and only track a photon in the vertical direction. Since the sun is about 150 million kilometers away from the ground, the solar flux from the sun is a parallel source. The solar irradiance is assumed to be unpolarized and unit strength photons from the infinite parallel source. The atmosphere is divided into a number of parallel zones. In Fig. 1, the observed radiance at a point O in the atmosphere is illustrated. The line of sight of the observer is expressed by the zenith angle θ and azimuthal angle ϕ. The solar radiation is considered to be an energy incident on the plane surface at zenith angle θ_0 with respect to the vertical direction. In the modeling of the ground, we use a Lambertian[19] surface in which the reflected incident radiation is uniformly distributed in all directions. When the photon collides with the planet surface, it is reflected according to Lambert's law.

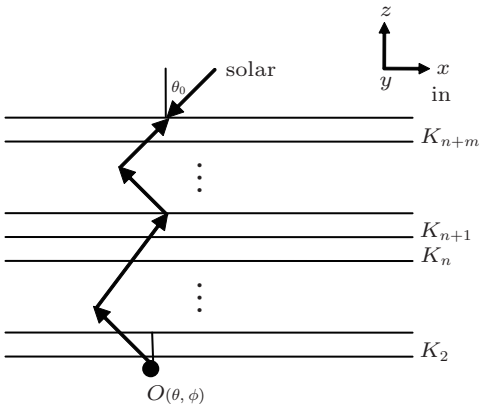


Fig. 1. Simulation geometry.

Before the first collision happens, the photons have two possible situations (downward and upward) to determine how far the photon can propagate. When the photon propagates downward, it cannot escape without scattering in the atmosphere nor from the ground. The optical depth that a photon can propagate is expressed as[20]

$$\tau = -\ln(\xi), \tag{7}$$

where ξ is a pseudo-random number distributed uniformly in the interval $(0, 1)$. Otherwise, the photon has a probability of escaping without collision. The optical depth due to collision is described by the following equation:[21]

$$\tau = -\ln(1 - \xi(1 - \exp(-\tau_{\max}))), \tag{8}$$

where $\tau_{\max}$ denotes the total optical path length through the atmosphere. The photon cannot pass through the atmosphere without collision, since $0 < \tau < \tau_{\max}$. Therefore, it increases the computational efficiency. In the meantime, the statistical weight of the photon is also adjusted to remove the bias by

$$w = w(1 - \exp(-\tau_{\max})), \tag{9}$$

where w denotes the photon weight. The distance d of the photon is calculated by the following equations:

$$d = \sum_k d_k, \tag{10}$$

$$\tau = \sum_k \beta_k d_k, \tag{11}$$

where k denotes the zones in which the photon will pass through, d_k the distance that the photon will pass through in zone k, and β_k the extinction coefficient for zone k. Each atmospheric zone has extinction coefficients including Rayleigh

β_{ray}, ozone β_{ozo}, and Heny–Greenstein β_{hen}. In each zone, $\beta_{ray}/(\beta_{ray}+\beta_{hen})$ is the probability of a Rayleigh scattering, $\beta_{hen}/(\beta_{ray}+\beta_{hen})$ is the probability of a Heny–Greenstein, $\beta_{ray}/(\beta_{ray}+\beta_{ozo})$ is the probability of absorption. Meanwhile, we also need to obtain the unit propagation direction vector of the photon. When we calculate the radiative transfer, the radiance is calculated by adding up the energy at each scattering point in the atmosphere and the radiance contribution from the ground. The radiance contribution consists of the Rayleigh and Henyey–Greenstein scatterings. The cosine of the scattering angle is completely determined by the direction vectors of the photon and solar flux. The scattering angle θ_{fs} is sampled by

$$\cos\theta_{fs} = -(a,b,c)\cdot(sa,sb,sc), \tag{12}$$

where (a,b,c) denotes the current direction vector for photon and (sa,sb,sc) represents the solar direction vector. The negative sign comes into being because the energy propagation direction is the same as the solar flux direction. Then, according to Eq. (6), we update the electric field and calculate the Stoke vector radiative transfer, where a clockwise rotation matrix of ϕ is expressed as[18]

$$R = \begin{pmatrix} \cos\phi & \sin\phi \\ -\sin\phi & \cos\phi \end{pmatrix}. \tag{13}$$

For the case of Rayleigh scattering, the scattering matrix is expressed as

$$M = \begin{pmatrix} \cos\theta_s & 0 \\ 0 & 1 \end{pmatrix}. \tag{14}$$

Equation (6) can be explicitly written in the following form for Rayleigh scattering:

$$\begin{pmatrix} E_1' \\ E_2' \end{pmatrix} = \begin{pmatrix} \cos\theta_s & 0 \\ 0 & 1 \end{pmatrix} \begin{pmatrix} \cos\phi & \sin\phi \\ -\sin\phi & \cos\phi \end{pmatrix} \begin{pmatrix} E_1 \\ E_2 \end{pmatrix}. \tag{15}$$

At each scattering event, the scattering angle cosine value is calculated, according to whether it is Rayleigh or Henyey–Greenstein.

The azimuthal angle ϕ in the interval $(0,\pi)$ is defined by

$$\phi = 2\pi\xi. \tag{16}$$

In the Rayleigh event, the scattering angle θ_s for an isotropic distribution is defined by

$$\cos\theta_s = 1-2\xi. \tag{17}$$

In the Heny–Greenstein event, the scattering angle θ_s is defined by

$$\cos\theta_s = \frac{1}{2g}\left[(1+g^2)-\left(\frac{1-g^2}{1+g-2g\xi}\right)^2\right], \tag{18}$$

where g denotes the anisotropic factor for the Heny–Greenstein function. Meanwhile, the photon direction deviates from the actual path and the energy is needed for the photon to go back to the detector. The direction vector for the photon will be updated when the photon passes through the atmosphere. The new direction vector for the photon is specified by

$$\begin{cases} a' = \left(\dfrac{ac\sin\theta\cos\phi - b\sin\theta\sin\phi}{\sqrt{1-c^2}}\right) + a\cos\theta, \\ b' = \left(\dfrac{bc\sin\theta\cos\phi + a\sin\theta\sin\phi}{\sqrt{1-c^2}}\right) + b\cos\theta, \\ c' = -\sqrt{1-c^2}\sin\theta\cos\phi + c\cos\theta, \end{cases} \tag{19}$$

where (a,b,c) and (a',b',c') denote the previous and present direction vectors of the photon, respectively, ϕ represents the azimuthal angle, and θ the scattering angle. Based on Eq. (14), the electric field is updated according to the updating rule of the electric field of scattered light. The event of scattering is simulated n times, then the present electric field is converted into the Stokes vector. A flow-chart that includes the main program is shown in Fig. 2. The states of photons are tracked step by step, the detailed description of the program is shown below.

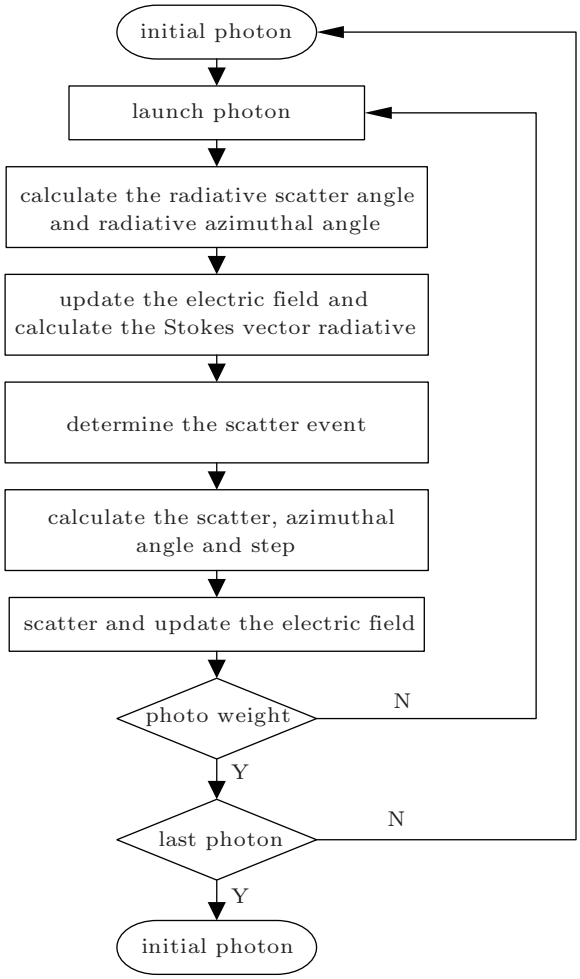


Fig. 2. Flow chart of REMC program of light in the atmosphere.

4. Results and discussion

Before performing the specific simulation, the accuracy of our REMC program should be verified. For Rayleigh scattering, our results are compared with the results tabulated by Kattawar and Adams[22] by employing an invariant imbedding technique with one layer, a wavelength of 0.65 μm, $\theta_s = 10.24°$, $\phi = 0.00°$, $w_0 = 0$, and an albedo of $A = 0.00$. Typical results of the comparison are shown in Figs. 3 and 4. The Stokes I and Q vectors at different values of optical depth τ, and the Stokes U vectors (the V component is always zero for pure Rayleigh scattering) at optical depth $\tau = 0.05$ are shown in Fig. 3. The degree of polarization and the relative error are shown in Fig. 4. From Figs. 3 and 4, we can clearly see that there is perfect agreement between REMC and the results from the invariant imbedding technique, and the verification

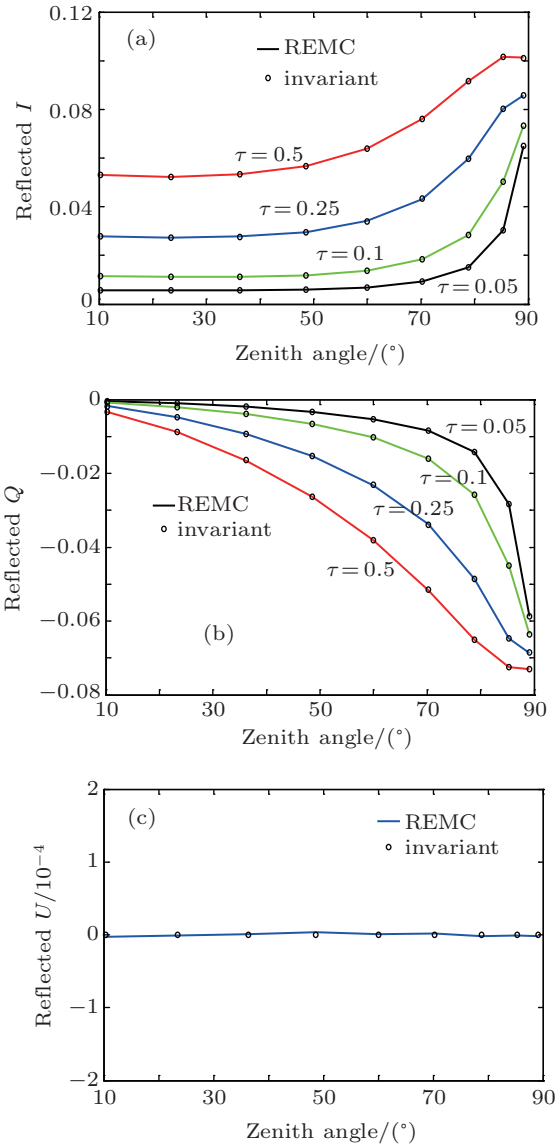


Fig. 3. (color online) Variations of (a) reflected I and (b) reflected Q of the REMC and the invariant imbedding with zenith angle at different values of optical depth, and variations of (c) the reflected U of the REMC and invariant imbedding at an optical depth of 0.05 with zenith angle.

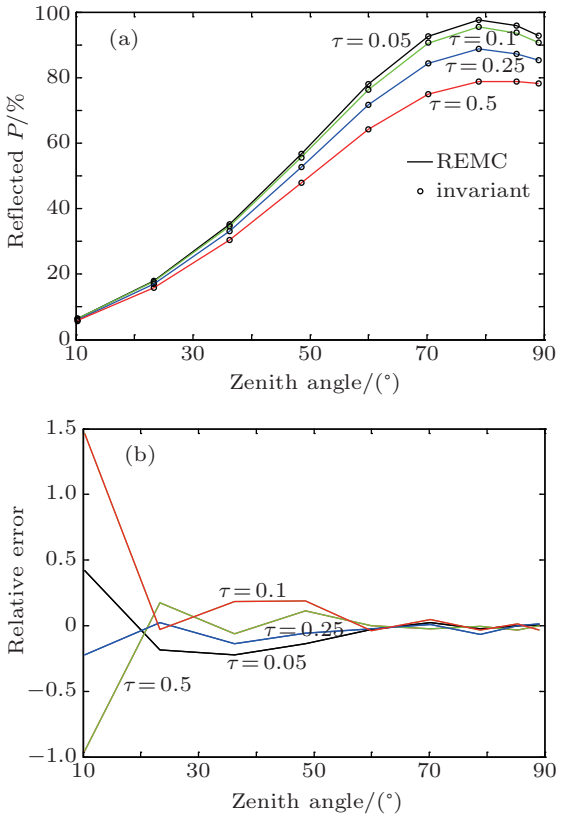


Fig. 4. (color online) Variations of (a) reflected P of the REMC and the invariant imbedding and (b) relative error of the two methods with zenith angle at different values of optical depth.

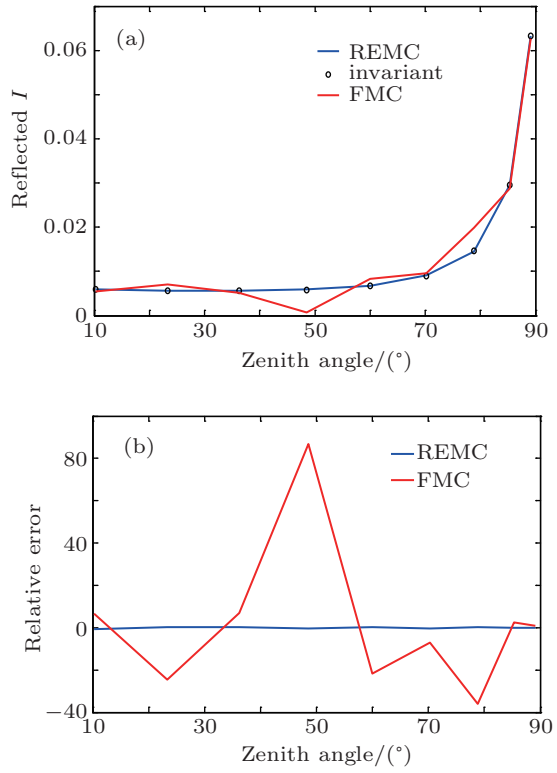


Fig. 5. (color online) Variations of (a) reflected I of the REMC, invariant imbedding, and FMC at an optical depth of 0.05 with zenith angle, and variations of (b) the relative error of the REMC and the FMC at an optical depth of 0.05 with zenith angle.

has shown the accuracy of our REMC program. In Fig. 4(b), we can see that when the number of photons is 10^6, the relative error is within 1.5%. Meanwhile, REMC has a very high efficiency. Based on the above condition, when the number of photons is 10^6, we compare the results from REMC and the Forward Monte Carlo (FMC) method[23] at an optical depth value of 0.05. From Fig. 5(a), we can find that the REMC method is better than the FMC method. In Fig. 5(b), the relative errors of the REMC and FMC are shown, respectively. We can clearly see that the FMC method is extremely inefficient when light is radiated onto a small spot. However, the REMC method is highly efficient. To further verify the efficiency of the REMC method, in Table 1, we show the reflected radiances for the numbers of photons being 10^4 and 10^5.

Table 1. Reflected radiances between REMC and invariant imbedding in different photon numbers.

	Invariant imbedding	Number = 10^4	Relative error	Number = 10^5	Relative error
10.24	0.005727	0.005842	–2.008032	0.005698	0.505151
23.36	0.005570	0.005434	2.447396	0.005604	–0.610413
36.23	0.005564	0.005629	–1.167505	0.005484	1.430445
48.54	0.005885	0.005677	3.529311	0.005810	1.269328
60.00	0.006872	0.006950	–1.138242	0.006870	0.035797
70.25	0.009267	0.009330	–0.684471	0.009346	–0.851947
78.85	0.015032	0.014878	1.027674	0.014979	0.351250
85.30	0.030438	0.029586	2.798541	0.030388	0.162921
89.09	0.065204	0.064546	1.008603	0.065091	0.174038

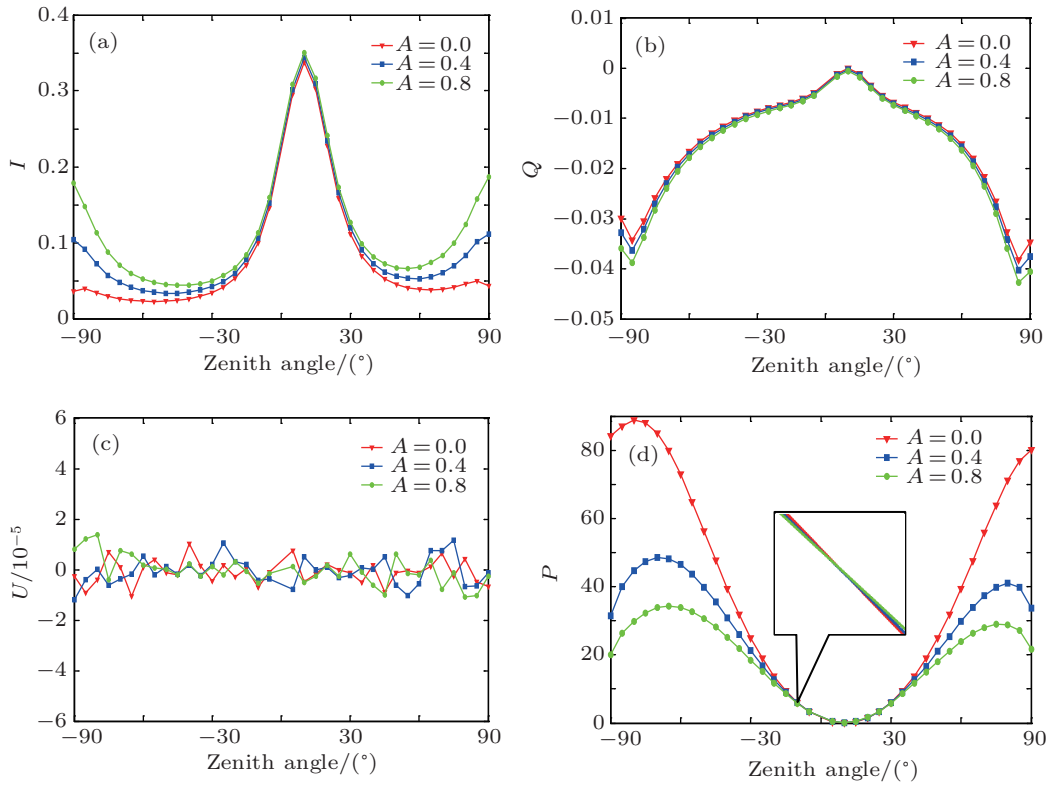


Fig. 6. (color online) Variations of transmitted radiance of Stokes (a) I, (b) Q, (c) U vectors, and (d) the degree of polarization with zenith angle at ground albedo values of 0.0, 0.4, and 0.8.

From Table 1, we can clearly see that when the numbers of the photons are 10^4 and 10^5, the relative errors are within 4% and 1.35%. It presents a high efficiency.

Next, we study the effects of the rough surfaces and optical depth by utilizing the REMC method. We use an atmospheric model, i.e., the earth atmosphere at a wavelength of 0.55 μm.[24] In this atmospheric model, there are 50 zones based on molecular scattering, aerosol scattering, and ozone absorption extinction, and the total optical depth value is 0.3035. In Fig. 6, we show the transmitted radiances of I,

Q, and U for Stokes vector and the degree of polarization (P) at the ground albedo values of 0.0, 0.4, and 0.8, $\theta_s = 10^\circ$ and $\tau = 0$. From Fig. 6, we clearly see that the value of I increases with the increase of the ground albedo, however, the value of Q decreases with the increase of the ground albedo. The ground albedo has no significant influence on U, but it has in influence on P. It should be noted that the ground albedo has a significant influence on P. Meanwhile, in Fig. 6(d), there are two special points where the degrees of polarization do not change with the ground albedo. When the zenith angle of the detector is laid between two points, P is proportional to the ground albedo. Otherwise, P is inversely proportional to the ground albedo.

Figures 7(a) and 7(b) show the zenith angles of the two points as a function of the solar zenith angle and a function of the optical depth of the detector location, respectively. From Fig. 7(a), we can see that the two points are almost symmetrical and the zenith angle corresponding to the axis of symmetry of the two points is the solar zenith angle. The distance between the two curves narrows in a solar zenith angle range from 10° to 50°, then widens with the increase of solar zenith angle. At a solar zenith angle of 80°, the negative sign comes into being because the zenith angle value of the point is larger than 90°. In Fig. 7(b), we can see that the zenith angles of one of the two points have no significant change with the optical depth of the detector.

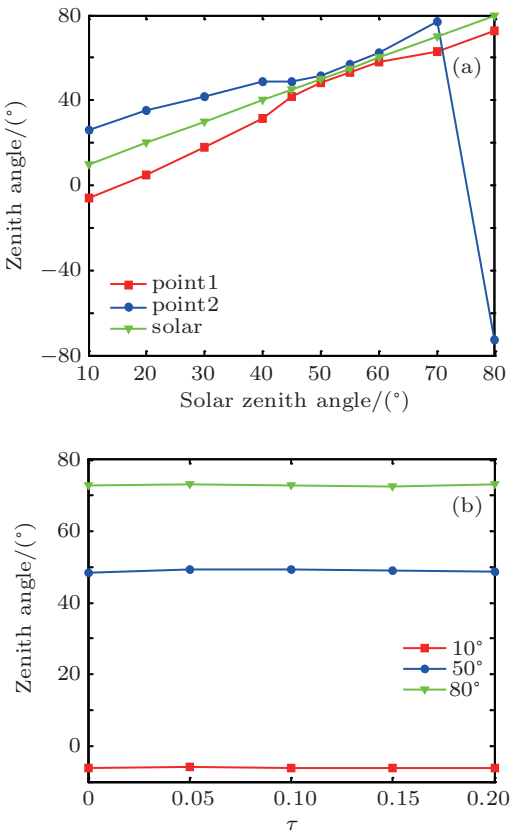


Fig. 7. (color online) Variations of zenith angles of the two points with (a) solar zenith angle and (b) optical depth.

Figure 8 shows the variations of the degree of polarization of a point with the optical depth of the detector at different ground albedo values. When the solar zenith angle is determined, comparing Fig. 8(a) with Fig. 8(b), the variations of the degree of polarization depend on the zenith angle of the detector location. Based on the above conclusions, we can find that two demarcation points are formed at the solar zenith angle $\theta_s = 10^\circ$. In Fig. 8, we find that when the zenith angle of the detector is between the two points, P is inversely proportional to the optical depth of the detector, the slope of the curve is relatively small. Otherwise, P is proportional to the optical depth of the detector and the slope of the curve is relatively large.

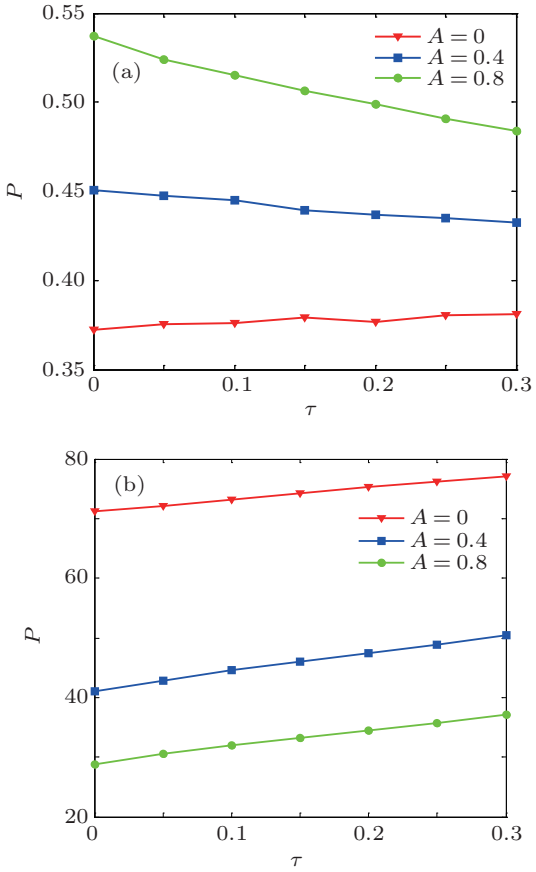


Fig. 8. (color online) Variations of the degree of polarization of a point with the optical depth of the detector at a solar zenith angle of 10° and at detector zenith angles of 5° (a) and 80° (b).

5. Conclusion

In this paper, a reverse electric field Monte Carlo method is proposed. The result shows that it is in good agreement with the result in the previous research. It presents a high efficiency shown in calculating the reflected radiance. Stokes vector and the degree of polarization are both numerically investigated. Simulation results demonstrate that there are two points, of which the degree of polarization is not influenced by the ground albedo nor the optical depth of the detector. The influences of the ground albedo and the optical depth of the

detector on the degree of polarization depend on the location of the zenith angle divided by the two points. Our results are crucial for polarization navigation in the near future, which can be used to analyze the influence of the zenith angle of the detector on the accuracy of navigation.

References

[1] Ramella-Roman J, Prahl S and Jacques S 2005 *Opt. Express* **13** 4420
[2] Ramella-Roman J, Prahl S and Jacques S 2005 *Opt. Express* **13** 10392
[3] Masrour R, Bahmad L and Benyoussef A 2013 *Chin. Phys. B* **22** 057504
[4] Xu Y D, Liu Q Q and Deng Y J 2012 *Chin. Phys. B* **21** 070211
[5] He B, Wang J G and Liu C L 2013 *Chin. Phys. B* **22** 073101
[6] Plass G N, Kattawar G W and Catchings F E 1973 *Appl. Opt.* **12** 314
[7] Kattawar G W 2013 *Appl. Opt.* **52** 940
[8] Adams C N and Kattawar G W 1978 *Icarus.* **35** 139
[9] Fischer J and Grassl H. 1984 *Appl. Opt.* **23** 1032
[10] Modest M F 2001 *Backward Monte Carlo Simulations in Radiative Heat Transfer* (Pennsylvania: Penn State University)
[11] Xu M 2004 *Opt. Express* **12** 6530
[12] Hayakawa C K, Potma E O and Venugopalan V 2011 *Biomed. Opt. Express* **2** 278
[13] Yun T, Zeng N, Li W, Li D, Jiang X and Ma H 2009 *Opt. Express* **17** 16590
[14] Chu J K, Zhao K C, Zhang Q and Wang T C 2007 *International Conference on Mechatronics and Automation*, August 5, 2007, Harbin, China, p. 3161
[15] Duan M Z and Guo X 2009 *Acta. Phys. Sin.* **58** 1353 (in Chinese)
[16] Chowdhary J, Cairns B and Travis L D 2006 *Appl. Opt.* **45** 5542
[17] Sun B, Wang H, Sun X B, S, Hong J and Zhang Y J 2012 *Chin. Phys. B* **21** 129501
[18] Sawicki J, Kastor N and Xu M 2008 *Opt. Express* **16** 5728
[19] Basri R and Jacobs D W 2003 *Pattern Analysis and Machine Intelligence* **25** 218
[20] Zhai P W, Kattawar G W and Yang P 2008 *Appl. Opt.* **47** 1037
[21] Roberti L 1997 *Appl. Opt.* **36** 7929
[22] Kattawar G W and Adams C N 1970 *J. Quant. Spectrosc. Radiat. Transfer* **10** 341
[23] Wang L H and Steven L J 1992 *Monte Carlo Modeling of Light Transport in Multi-layered Tissues in Standard C* (Vol. 1) (Houston: M. D. Anderson Cancer Center Press) pp. 1–173
[24] Elterman L 1968 *Air Force Cambridge Research Labs Hanscom AFB MA* **68** 0153